Three-body Faddeev-Alt-Grassberger-Sandhas approach to direct nuclear reactions

A. Deltuva and A. C. Fonseca
Centro de Física Nuclear da Universidade de Lisboa, P-1649-003 Lisboa, Portugal
(Received 30 October 2008; published 14 January 2009)

Momentum-space three-body Faddeev-like equations are used to calculate elastic, transfer, and charge-exchange reactions resulting from the scattering of deuterons on ^{12}C and ^{16}O or protons on ^{13}C and ^{17}O, with ^{12}C and ^{16}O treated as inert cores. All possible reactions are calculated in the framework of the same model space. Comparison with previous calculations based on approximate methods used in nuclear reaction theory is made.

DOI: 10.1103/PhysRevC.79.014606 PACS number(s): 24.10.Eq, 24.50.+g, 25.55.Ci, 25.55.Hp

I. INTRODUCTION

As discussed in the review article by Austern *et al.* [1] twenty years ago, three-body models of deuteron-induced reactions became important since the early studies of stripping theory [2], where "the internal coordinates of the target nucleus are ignored and the only dynamically active variables are the coordinates, relative to the target nucleus, of the interacting nucleon that is captured by the nucleus and the spectator nucleon that goes on to the detector."

The present work goes back in time, recaptures the three-body concept of direct nuclear reactions that is common to continuum discretized coupled channels (CDCC) calculations [1], and shows the results obtained by solving Faddeev/Alt, Grassberger, and Sandhas (AGS) equations [3–5] for elastic, transfer, and breakup reactions where three-body dynamics plays a dominant role. In this work we attempt to calculate all observables using dynamical models based on energy-independent or energy-dependent optical potentials for the nucleon-nucleus interaction [6] and realistic neutron-proton (np) potentials such as CD-Bonn [7]. Some examples are shown for reactions initiated by deuterons on ^{12}C and ^{16}O, as well as protons on ^{13}C and ^{17}O. Although the use of energy-dependent potentials in three-body calculations is not free of theoretical problems that are discussed in the following, the results we show demonstrate the possibilities and the shortcomings of this model; this is, above all, the aim of the present paper. In addition, we present the exact derivation of an alternative set of equations that may serve as the basis for future investigations on improving approximate methods in nuclear reaction theory.

Although deuteron-nucleus three-body models, including striping or pickup, have already been explored in the past in the framework of Faddeev/AGS equations starting with the pioneering work of Aaron and Shanley [8] to the more recent calculations of Alt *et al.* [9], all of them were drastically simplified. In most cases separable interactions were used between pairs and the correct treatment of the Coulomb interaction was missing. This situation has now changed owing to recent progress in the description of proton-deuteron elastic scattering and breakup [10,11], where the Coulomb repulsion is fully included by using the method of screening and renormalization [12,13] together with realistic nuclear potentials. This technical development was applied to three-body nuclear reactions to test the accuracy of the CDCC method [14] and the convergence of the multiple scattering series in the framework of the Glauber approximation [15] and distorted-wave impulse approximation (DWIA) [16], which are standard approximations used to describe nuclear reaction data.

Some of the interaction models employed in this work and in CDCC calculations are formally identical, but instead of solving the three-body Schrödinger equation in coordinate space using a representation in terms of a set of eigenstates pertaining to a given subsystem Hamiltonian, we solve the Faddeev/AGS equations in momentum space and obtain a numerically well converged solution of the three-body problem for all reactions allowed by the chosen interactions. In Ref. [14] we benchmarked the two methods and concluded that CDCC is indeed a reliable method to calculate deuteron-nucleus elastic and breakup cross sections but may not provide a sufficiently accurate solution of the three-body problem for transfer and breakup in one-neutron halo nucleus scattering from a proton target such as in ^{11}Be + p reactions. In those cases the comparison of CDCC results with experimental data may be misleading.

In Sec. II we recall the Faddeev/AGS equations, in Sec. III we present the results for three dynamical models, and in Sec. IV we compare them with the results of standard approximations used in nuclear reaction theory. Conclusions are given in Sec. V.

II. THE THREE-BODY EQUATIONS

Let us consider a system of three particles ($\alpha = 1, 2, 3$) with kinetic energy operator H_0, interacting by means of two-body potentials v_α ($v_1 = v_{23}$ in the standard odd-man-out notation). The full resolvent

$$G(Z) = \left(Z - H_0 - \sum_\sigma v_\sigma \right)^{-1} \tag{1}$$

and the channel resolvent

$$G_\alpha(Z) = (Z - H_0 - v_\alpha)^{-1} \tag{2}$$

may be related through the AGS transition operator $U_{\beta\alpha}(Z)$ as

$$G(Z) = \delta_{\alpha\beta}\, G_\alpha(Z) + G_\beta(Z) U_{\beta\alpha}(Z) G_\alpha(Z). \tag{3}$$

The transition operator $U_{\beta\alpha}(Z)$ satisfies the AGS equation [4]

$$U_{\beta\alpha}(Z) = \bar{\delta}_{\beta\alpha} G_0^{-1}(Z) + \sum_{\sigma} \bar{\delta}_{\beta\sigma} T_\sigma(Z) G_0(Z) U_{\sigma\alpha}(Z), \quad (4)$$

where the summation on σ runs from 1 to 3, $\bar{\delta}_{\beta\alpha} = 1 - \delta_{\beta\alpha}$, $G_0(Z) = (Z - H_0)^{-1}$ is the free resolvent, and $T_\alpha(Z)$ is the two-body transition matrix (t matrix) that obeys the Lippmann-Schwinger equation for pair α,

$$T_\alpha(Z) = v_\alpha + v_\alpha G_0(Z) T_\alpha(Z). \quad (5)$$

At a given energy E in the three-body center-of-mass (c.m.) system the on-shell matrix elements $\langle \psi_\beta | U_{\beta\alpha}(E + i0) | \psi_\alpha \rangle$ calculated between the appropriate channel states yield all the relevant elastic, inelastic, and transfer ($\beta, \alpha = 1, 2, 3$) as well as breakup ($\beta = 0$) amplitudes. The channel state $|\psi_\alpha\rangle$ for $\alpha = 1, 2, 3$ is the eigenstate of the corresponding channel Hamiltonian $H_\alpha = H_0 + v_\alpha$ with the energy eigenvalue E comprising the bound state wave function for pair α times a relative plane wave between particle α and pair α. For breakup the final state is a product of two plane waves, corresponding to the relative motion of three free particles.

The AGS equations [Eq. (4)] are Faddeev-like equations with compact kernel and therefore suitable for numerical solution; they are consistent with the corresponding Schrödinger equation and therefore provide an exact description of the quantum three-body problem. After partial wave decomposition Eq. (4) becomes a two-variable integral equation, which we solve by standard discretization of momentum variables and summation of the multiple scattering series by the Padé method; more details can be found in Refs. [17,18]. As in all numerical calculations, convergence of results has to be tested with respect to the number of included partial waves, mesh points, and Padé steps.

To include the Coulomb interaction between two charged particles we use the method of screening and renormalization [10,12,13]. The Coulomb potential is screened, standard scattering theory for short-range potentials is used in the form of Eq. (4) with parametric dependence on the screening radius R, and the renormalization procedure is applied to obtain R-independent results for sufficiently large R, which correspond to the unscreened limit. A complete review on this subject is presented in Ref. [19] together with a number of practical applications.

III. THE DYNAMICAL MODELS

In this section we set the three-body dynamics we apply to study all the reactions initiated by deuterons on ^{12}C and ^{16}O as well as protons on ^{13}C and ^{17}O, where ^{12}C and ^{16}O are considered as inert cores.

Although in most nuclear reaction calculations the deuteron wave function is generated through a Gaussian potential fitted to the deuteron binding energy, which is then used to drive the np interaction in all other partial waves, we use the CD-Bonn [7] potential as our realistic interaction for all np partial waves including the deuteron channel.

For the neutron-nucleus (nA) and proton-nucleus (pA) interactions we use the optical potentials of Watson *et al.* [6], which are based on an optical model analysis of nucleon scattering from $1p$-shell nuclei between 10 and 50 MeV; the nucleus A is a structureless core of mass number A. Although core excitation may be treated in the present three-body models, we discard such a possibility at this time. Therefore the relevant parameters of this optical model fit are both energy and mass dependent and are fitted to the existing data over the energy and mass range. For specific nuclei and energy, one could perhaps obtain a better fit but, as mentioned in Sec. I, our goal is to explore the possibilities of a three-body model that can simultaneously describe all reactions allowed by the chosen interactions and leave the fine-tuning for an improved model study. In all calculations nucleons are considered as spin-1/2 particles and the nuclear cores as spin-0 particles; the spin-orbit terms of the optical potentials are included as well as the full operator structure of the CD-Bonn potential for the np pair. The calculations include np partial waves with total angular momentum $I \leqslant 3$, nA partial waves with orbital angular momentum $L \leqslant 8$, and pA partial waves with $L \leqslant 20$; the total three-particle angular momentum is $J \leqslant 35$. Depending on the reaction and energy, some of these quantum number cutoffs can be safely chosen significantly lower, leading, nevertheless, to well-converged results. The pA channel is more demanding than the nA channel because of the screened Coulomb force, where the screening radius $R \approx 10$ fm for the short-range part of the scattering amplitude is sufficient for convergence. The only exception are reactions leading to a final (Ap) bound state where $R \approx 15$ fm and a sharper screening is needed. With this choice of the calculational parameters we obtain well-converged results for all considered observables such that all discrepancies with the experimental data can be attributed solely to the shortcomings of the interaction models that are used.

A. Model 1: Energy-independent optical potentials

In this case we use the traditional approach based on energy-independent optical potentials whose parameters are chosen at a fixed energy. For deuteron scattering from nucleus A the parameters for the nA and pA potentials are taken from Ref. [6] at half the laboratory energy of the deuteron projectile. For proton scattering from the (An) nucleus the pA parameters are taken from Ref. [6] at the laboratory energy of the proton beam and the nA parameters at zero energy, where the imaginary part of the nA optical potential is zero. Small adjustments to these nA parameters are made to be able to reproduce the experimental binding energies of the ground and excited single-particle states of the (An) nucleus while all Pauli forbidden bound states of the resulting potential are removed as described in Ref. [20]. Original [6] and adjusted values of these parameters are given in Table I. In the present model only the modified nA parameters are used in given partial waves, leading to the single-particle states listed in Table II for ^{13}C and ^{17}O; in all other nA partial waves we used the original parameters [6] as well as for the pA optical potential. Whereas in $d + A$ scattering the pA and nA potentials are complex, in $p + (An)$ scattering only the pA potential is complex.

TABLE I. Original parameters of the real part of the nucleon-nucleus optical potential [6] (first line) and those adjusted to the energies of bound states or resonances in given partial waves, all in units of MeV. The strength of the central part is related to v_R as $V_R = v_R + 0.4ZA^{-1/3} \pm 27.0(N-Z)/A - 0.3E_{\rm c.m.}\Theta(E_{\rm c.m.})$ and $V_{\rm so}$ is the strength of the spin-orbit part; see Ref. [6] for more details.

	$v_R(nA)$	$v_R(pA)$	$V_{\rm so}(nA)$	$V_{\rm so}(pA)$
Ref. [6]	60.00	60.00	5.5	5.5
N-^{12}C (s)	67.50	66.47		
N-^{12}C (p)	61.67	61.50	20.38	20.83
N-^{12}C (d)	66.42	66.42	5.5	5.5
N-^{16}O (s)	61.65	60.94		
N-^{16}O (d)	61.47	60.89	5.4	5.4

Although in both cases we are dealing with the same particles, the Hamiltonians are different and, therefore, in $d + A$ we cannot calculate $d + A \to p + (An)$, but in $p + (An)$ we can calculate the inverse reaction $p + (An) \to d + A$, or even $p + (An) \to p + (An)^*$, because the nA interaction is real, in contrast to $d + A$ where it is complex.

Results for these studies are shown by the dotted curves (M1) in Figs. 1–3 for $d + {}^{12}$C and $p + {}^{13}$C and in Figs. 4–6 for $d + {}^{16}$O and $p + {}^{17}$O at different energies. As previously mentioned the results shown by the dotted curves in Fig. 1 (Fig. 4) are obtained with a different Hamiltonian from those in Figs. 2 and 3 (Figs. 5 and 6). In general the description of the data for elastic scattering is fairly reasonable and within what can be expected from corresponding CDCC calculations. For the transfer reactions $p + {}^{13}\text{C} \to d + {}^{12}\text{C}$ and $p + {}^{17}\text{O} \to d + {}^{16}\text{O}$ shown in Figs. 3 and 4, respectively, one gets a reasonable agreement with data in the forward direction (except for a scaling factor), but deviations from data increase for $\Theta_{\rm c.m.} > 30^\circ$.

The fact that traditional three-body models of $d + A$ and $p + (An)$ scattering are inconsistent with each other encouraged us to study other possibilities to shed light on the sensitivity of results to different dynamical approaches.

B. Model 2: Energy-dependent optical potentials

The two-body t matrix given by Eq. (5) enters the Faddeev/AGS equation [Eq. (4)] for the transition operator $U_{\beta\alpha}(Z)$. Even if the potential is energy independent, the pair t matrix has to be calculated at the two-body energies

TABLE II. Binding energies (in MeV) of the bound states corresponding to the potential parameters of Table I. Pauli forbidden bound states that are removed are marked with *.

	$1s_{1/2}$	$2s_{1/2}$	$1p_{3/2}$	$1p_{1/2}$	$1d_{5/2}$
^{13}C	38.022*	1.857	18.722*	4.946	1.092
^{13}N	33.864*		15.957*	1.944	
^{17}O	37.213*	3.272	19.267*	16.067*	4.143
^{17}F	32.559*	0.105	15.561*	12.348*	0.600

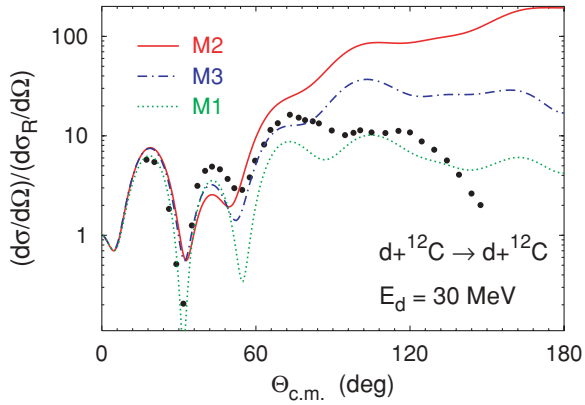

FIG. 1. (Color online) Differential cross section divided by Rutherford cross section for $d + {}^{12}$C elastic scattering at $E_d = 30$ MeV. Predictions of Model 1 (dotted curve), Model 2 (solid curve), and Model 3 (dashed-dotted curve) are compared with the experimental data from Ref. [21].

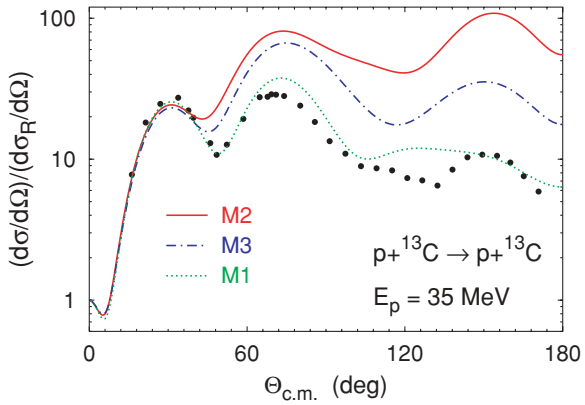

FIG. 2. (Color online) Differential cross section divided by Rutherford cross section for $p + {}^{13}$C elastic scattering at $E_p = 35$ MeV. Curves are as in Fig. 1. The experimental data are from Ref. [22].

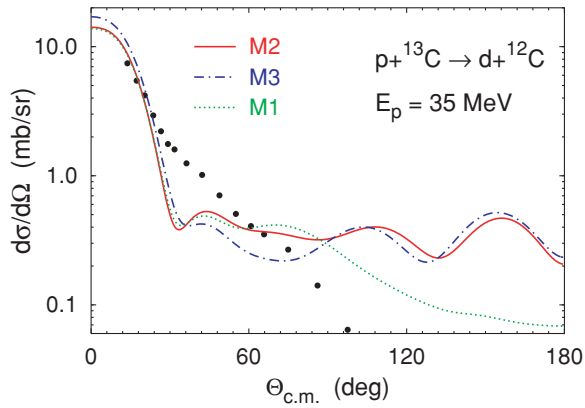

FIG. 3. (Color online) Differential cross section for $p + {}^{13}\text{C} \to d + {}^{12}$C transfer at $E_p = 35$ MeV. Curves are as in Fig. 1. The experimental data are from Ref. [23].

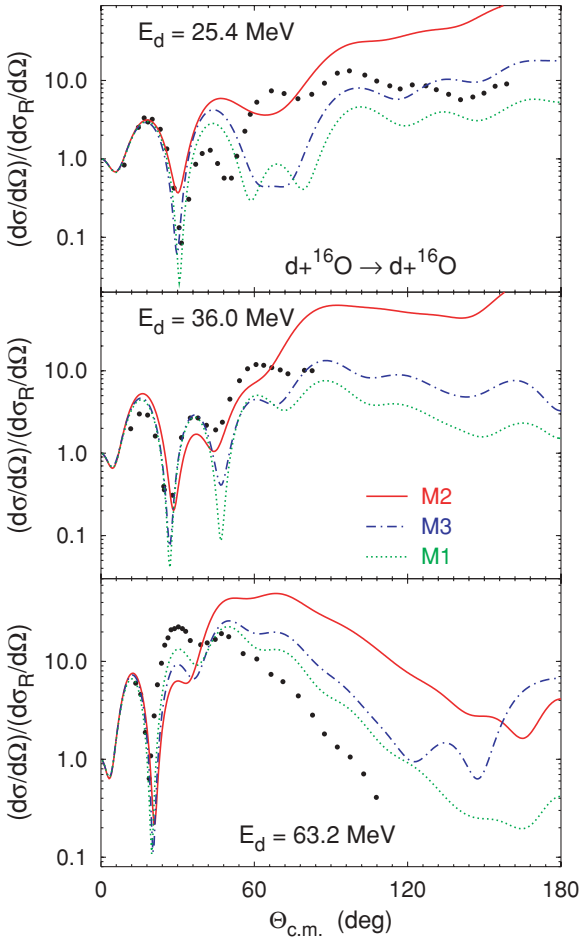

FIG. 4. (Color online) Differential cross section divided by Rutherford cross section for $d + {}^{16}\mathrm{O}$ elastic scattering at $E_d =$ 25.4, 36.0, and 63.2 MeV. Curves are as in Fig. 1. The experimental data are from Refs. [24,25].

$e = E - q_\alpha^2/2\mu_\alpha$, where q_α is the relative momentum between particle α and the c.m. of pair α that has to be integrated over when solving the Faddeev/AGS equation, μ_α is the

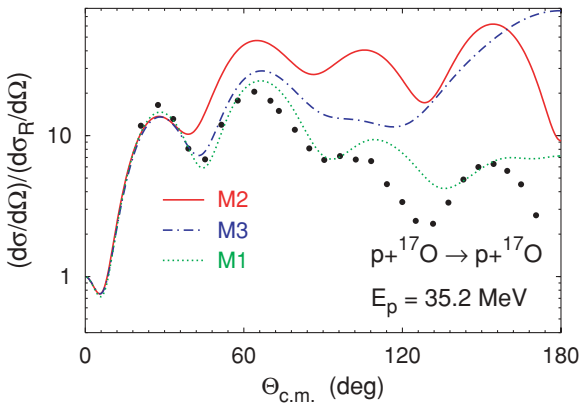

FIG. 5. (Color online) Differential cross section divided by Rutherford cross section for $p + {}^{17}\mathrm{O}$ elastic scattering at $E_p =$ 35.2 MeV. Curves are as in Fig. 1. The experimental data are from Ref. [22].

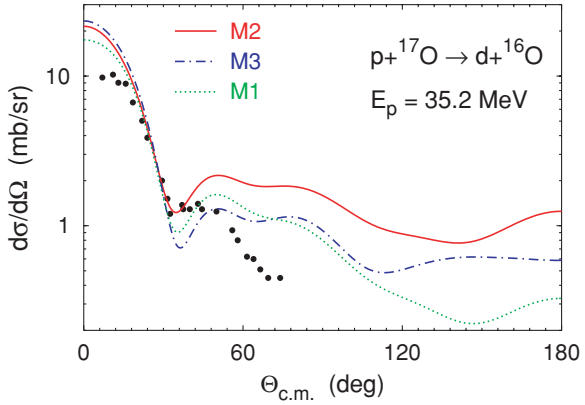

FIG. 6. (Color online) Differential cross section for $p + {}^{17}\mathrm{O} \rightarrow d + {}^{16}\mathrm{O}$ transfer at $E_p = 35.2$ MeV. Curves are as in Fig. 1. The experimental data are from Ref. [24].

corresponding particle-pair α reduced mass, and E is the three-body energy in the c.m. system. Therefore in three-body calculations the particles in all pairs scatter at two-body energies between E and $-\infty$. In the case of the CD-Bonn potential np observables are described with $\chi^2/\mathrm{datum} \sim 1$ from zero np relative energy to the π production threshold. The same cannot be said about the nA and pA optical potentials, which in the previous model were chosen at a fixed energy. Hence they describe the corresponding data at that energy but not over the broader range that is relevant for the solution of the three-body Faddeev/AGS equation.

In the present model we take the full energy dependence of the optical potential such that when nA or pA pairs interact at a given positive relative energy, the used parameters of the optical potential fit elastic nA and pA scattering at that energy. In addition, when the energy becomes negative the corresponding potentials become real and energy-independent and support a number of bound states that correspond to the ground and excited states of the (An) and (Ap) nucleus whereas the Pauli forbidden states are removed. As mentioned before, the parameters of the energy-dependent optical potentials are slightly modified to obtain the experimental binding energies at zero energy, as indicated in Table I for both nA or pA potentials in given partial waves. In addition, the binding energy of the Pauli forbidden $1p_{3/2}$ state in $^{13}\mathrm{C}$ and $^{13}\mathrm{N}$ systems is fitted to the $^{12}\mathrm{C}$ neutron and proton separation energy, respectively, whereas the $1p_{1/2}$ binding energy in $^{17}\mathrm{O}$ and $^{17}\mathrm{F}$ systems calculated with original parameters [6] is close to the corresponding nucleon separation energies of $^{16}\mathrm{O}$. The resulting binding energies are given in Table II for $^{13}\mathrm{C}$, $^{13}\mathrm{N}$, $^{17}\mathrm{O}$, and $^{17}\mathrm{F}$ nuclei. In the case of N-$^{12}\mathrm{C}$, where the adjusted parameters are quite different from the original ones, at positive energies v_R is replaced by $v_R(E_{\mathrm{c.m.}}) = 60.0 + (v_R - 60.0)\exp(-E_{\mathrm{c.m.}}/2)$ and V_{so} is replaced by $V_{\mathrm{so}}(E_{\mathrm{c.m.}}) = 5.5 + (V_{\mathrm{so}} - 5.5)\exp(-E_{\mathrm{c.m.}}/2)$, such that the potential preserves the description of the N-$^{12}\mathrm{C}$ scattering data in the desired energy regime and remains a continuous function of the energy. Such a replacement is not needed in the case of N-$^{16}\mathrm{O}$, where the adjusted parameters are very close to the original ones.

Using energy-dependent pair interactions in three-body calculations is by no means free of theoretical complications, such as the problem of nonorthogonality of three-body wave functions at different energies as a result of the absence of a Hamiltonian theory for the scattering process. This issue can be easily understood even at the two-body level. If the potential is energy dependent the two-body bound states and scattering states are not necessarily orthogonal, much like scattering states corresponding to different energies. Therefore completeness relations and three-particle unitarity may be at fault even in the presence of real interactions. Nevertheless, present optical model fits, in particular the one by Watson *et al.*, are rather weak in their energy dependence, as can be seen by the strength of the energy-dependent coefficients compared with the energy-independent parameters; furthermore, this energy dependence is smooth over the energy range of the fit except perhaps for the N-^{12}C spin-orbit interaction in p waves near $e = 0$. Even in this case we tried different p-wave interactions and the results are not very different, as demonstrated in the Appendix. For this reason we believe that the problems of nonorthogonality of wave functions and completeness may be sufficiently small to allow a serious consideration of this model given its notorious advantages such as consistent dynamics for both $d + A$ and $p + (An)$ scattering and the possibility of calculating transfer reactions to $p + (An)$ and $n + (Ap)$ final states.

Furthermore, one should keep in mind that the energy dependence and the imaginary part of the optical potential have the same origin; they arise after the elimination of active degrees of freedom (i.e., excitations, multiconfiguration mixing, and breakup of nucleus A) from the considered Hilbert space, as described earlier by Feshbach [26]. However, in a three-body system this leads in addition to an effective energy-dependent complex three-body potential, or, in general, to many-body potentials (up to n-body) in an n-body system, as formally developed by Polyzou and Redish [27] in the framework of exact n-body theory. Well-known examples are the three- and four-nucleon systems described within the interaction model with energy-independent two-body potentials allowing for an explicit excitation of a nucleon to a Δ isobar [28,29], which yields effective energy-dependent two-nucleon and many-nucleon forces that are mutually consistent. In the study of three-nucleon observables it was found that the Δ-isobar effect of the two-nucleon nature is often overcompensated by the three-nucleon force effect. Thus, also in the three-body nuclear reactions one could expect a similar situation for some observables, that is, a partial cancellation of the effects arising from the energy dependence of the two-body potential and from the three-body potential if the latter would be included in the calculations. However, when the energy dependence of the two-body optical potential is introduced in the usual phenomenological way, it is not clear what the consistent three-body potential should be. We therefore do not attempt to include an optical three-body potential in the present calculations, although such an extension of the Faddeev/AGS framework is possible.

In Figs. 1–11 the solid curves (M2) show the results of the present fully energy dependent model for all possible reactions at different energies. A number of interesting features emerge:

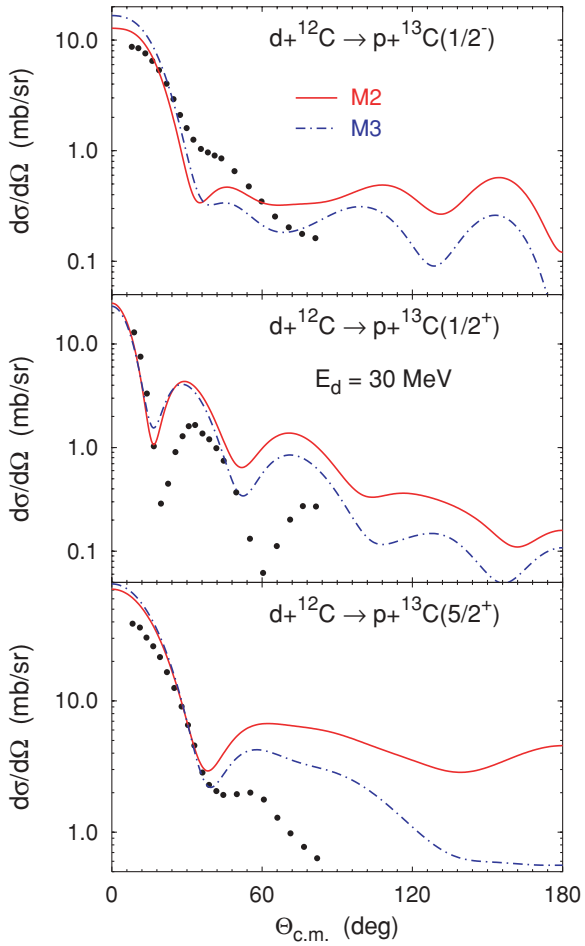

FIG. 7. (Color online) Differential cross section for $d + {}^{12}\mathrm{C} \to p + {}^{13}\mathrm{C}$ transfer at $E_d = 30$ MeV. Predictions of Model 2 (solid curve) and Model 3 (dashed-dotted curve) are compared with the experimental data from Ref. [30].

(i) Elastic scattering results shown in Figs. 1, 2, 4, and 5 differ quite strongly from Model 1 (dotted curves), particularly at large angles, and become considerably worse when compared to data.

(ii) In the low angular region ($\Theta_{\mathrm{c.m.}} < 30^\circ$) $p + {}^{13}\mathrm{C} \to d + {}^{12}\mathrm{C}$ (Fig. 3) and $p + {}^{17}\mathrm{O} \to d + {}^{16}\mathrm{O}$ (Fig. 6) results are very similar to those obtained with Model 1, except for a small scaling factor.

(iii) Figure 7 shows new results for the transfer reactions $d + {}^{12}\mathrm{C} \to p + {}^{13}\mathrm{C}$ to ground state $1/2^-$ and excited states $1/2^+$ and $5/2^+$. Again up to $\Theta_{\mathrm{c.m.}} \simeq 30^\circ$ the calculation follows the data within a small scaling coefficient that may be associated with a spectroscopic factor. In the case of the transfer to the ground state, the solid curves in Figs. 3 and 6 have similar shape, as expected by detailed balance taking into account the small difference in the energies. The calculations also reflect the qualitative features of the data.

(iv) Figures 9 and 10 show new results for the transfer reactions $d + {}^{16}\mathrm{O} \to p + {}^{17}\mathrm{O}$ to ground state $5/2^+$ and excited state $1/2^+$. Again the calculations describe the

qualitative features of the data though scaling factors may be needed.

(v) Figures 8 and 11 show new results for $p + {}^{13}\mathrm{C} \to n + {}^{13}\mathrm{N}$ ground state $1/2^-$ and $p + {}^{17}\mathrm{O} \to n + {}^{17}\mathrm{F}$ ground state $5/2^+$ and excited state $1/2^+$. Although in the charge-exchange reactions to the ground state the data are not described successfully, it is worth noting that in the $p + {}^{17}\mathrm{O} \to n + {}^{17}\mathrm{F}$ excited state $(1/2^+)$ the calculations are in very reasonable agreement with data, except for a small scaling factor.

It is worth noting at this point that a good description of elastic data beyond small angles does not seem to be necessary to get the right magnitude of the transfer cross sections at small angles since Figs. 3 and 6 show similar results for two distinct models that lead to very different results for the elastic cross sections at large angles (see Figs. 1, 2, 4, and 5).

C. Model 3: A "hybrid" optical potential approach

Having studied these two extreme dynamical model approaches, the energy-independent and the fully energy dependent, we attempt to study a combination of the two. Since we want the relevant nuclei, ^{13}C, ^{13}N, ^{17}O, and ^{17}F, to have the proper low-energy spectra to describe all the relevant transfer reactions discussed before, we use in this case a partial-wave-dependent optical potential in the following way: (a) For $d + A$ reactions in N-^{12}C (N-^{16}O) s, p, and d waves (s and d waves) we use the energy-dependent optical potentials of Model 2; for $p + (An)$ reactions the pA potential in these partial waves is energy dependent as well, but the nA potential is taken over from Model 1 since it is sufficient to bind ^{13}C and ^{17}O. (b) In all other partial waves we use the energy-independent optical potentials of Model 1 with a few nuances that are explained in the text, depending on whether we have $d + A$ or $p + (An)$ scattering.

Since Model 1 is more absorptive than Model 2 owing to the large impact of the imaginary part of the optical interactions on the elastic cross sections we expect this hybrid model to improve the description of the elastic data.

For $d + A$ scattering, results are shown by the dash-dotted curves (M3) in Figs. 1, 4, 7, 9, and 10. In $d + {}^{12}\mathrm{C}$ ($d + {}^{16}\mathrm{O}$) both nA and pA optical potentials are, as in Model 2, energy dependent in s, p, and d waves (s and d waves) but in all other partial waves they are energy independent with the parameters chosen at half the deuteron laboratory energy, as in Model 1. The dash-dotted curves show a remarkable improvement compared with the fully energy dependent calculations (solid lines in Model 2), particularly at large angles. This effect is visible not only in elastic scattering (Figs. 1 and 4) but also in the transfer reactions $d + A \to p + (An)$ shown in Figs. 7, 9, and 10, where in some specific cases such as in Figs. 9 and 10 one gets quite reasonable descriptions of the data.

For $p + (An)$ scattering results are again shown in Figs. 2, 3, 5, 6, 8, and 11 by the dash-dotted curves (M3). In $p + {}^{13}\mathrm{C}$ ($p + {}^{17}\mathrm{O}$) the pA optical potentials are, as in Model 2, energy dependent in s, p, and d waves (s and d waves) and, in all other partial waves, are energy independent with the parameters chosen at the proton laboratory energy, as in Model 1. As for the nA optical potential it is chosen as in Model 1, where in all partial waves the potential is real and supports a number of single-particle states as mentioned before. As in $d + A$ reactions, we notice an improvement in the description of $p + (An)$ elastic (Figs. 2 and 5) as well as $p + (An) \to d + A$ transfer (Figs. 3 and 6) observables. Nevertheless, at small angles ($\Theta_{\mathrm{c.m.}} \leqslant 30^\circ$), the differences among Models 1, 2, and 3 are quite small, indicating that the extracted spectroscopic factors would be of similar size as well.

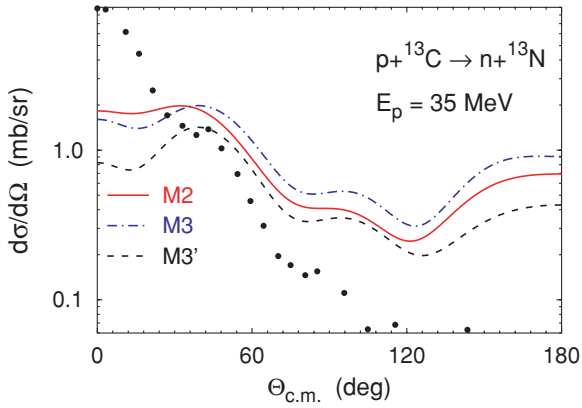

FIG. 8. (Color online) Differential cross section for the $p + {}^{13}\mathrm{C} \to n + {}^{13}\mathrm{N}$ reaction at $E_p = 35$ MeV. The dashed curve is the prediction of Model 3′; other curves are as in Fig. 7. The experimental data are from Ref. [31].

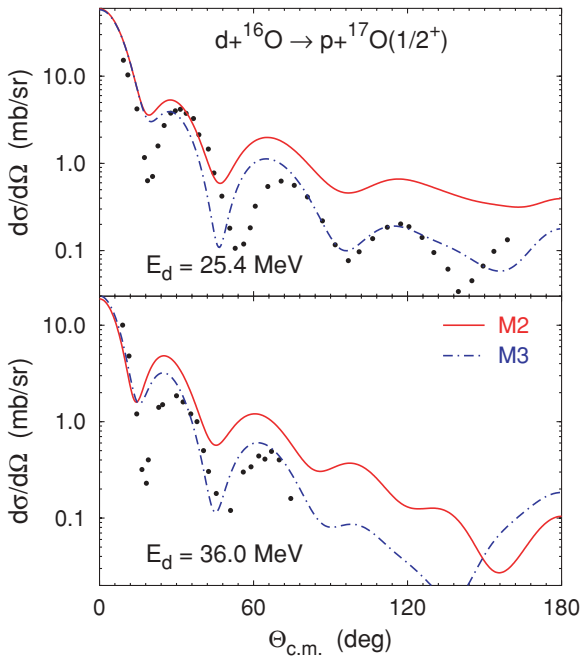

FIG. 9. (Color online) Differential cross section for $d + {}^{16}\mathrm{O} \to p + {}^{17}\mathrm{O}$ transfer at $E_d = 25.4$ and 36.0 MeV. Curves are as in Fig. 7. The experimental data are from Ref. [24].

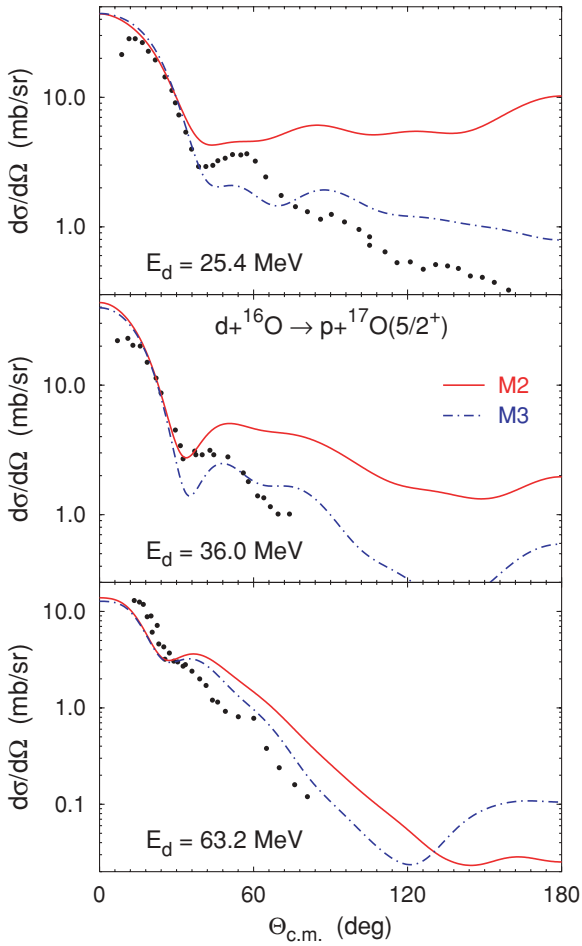

FIG. 10. (Color online) Differential cross section for $d + {}^{16}\mathrm{O} \to p + {}^{17}\mathrm{O}$ transfer at $E_d = 25.4$, 36.0, and 63.2 MeV. Curves are as in Fig. 7. The experimental data are from Ref. [24].

Finally, for the charge-transfer reactions shown in Figs. 8 and 11 we add a new calculation shown by the dashed curves (M3′), where the nA optical potential is energy dependent in the s, p, and d partial waves for ^{13}C and in the s and d waves for ^{17}O as in Model 2 but is, in the other partial waves, energy independent with the parameters chosen according to the laboratory energy of the neutron in the inverse reaction $n + (Ap) \to p + (An)$. The three curves shown in Figs. 8 and 11 are not very different aside from a scaling factor.

IV. DISTORTED WAVE EQUATIONS

To relate our calculations to the standard approaches of nuclear reaction theory we derive an alternative set of scattering equations. Introducing an effective interaction $\tilde{V}_\alpha$ acting between particle α and the c.m. of pair α as shown in Fig. 12 one may define a new resolvent

$$\tilde{G}_\alpha(Z) = (Z - H_0 - v_\alpha - \tilde{V}_\alpha)^{-1}, \tag{6}$$

such that

$$\tilde{G}_\alpha(Z) = G_\alpha(Z) + G_\alpha(Z)\,\tilde{T}_\alpha(Z)\,G_\alpha(Z), \tag{7}$$

$$\tilde{T}_\alpha(Z) = \tilde{V}_\alpha + \tilde{V}_\alpha\,G_\alpha(Z)\,\tilde{T}_\alpha(Z). \tag{8}$$

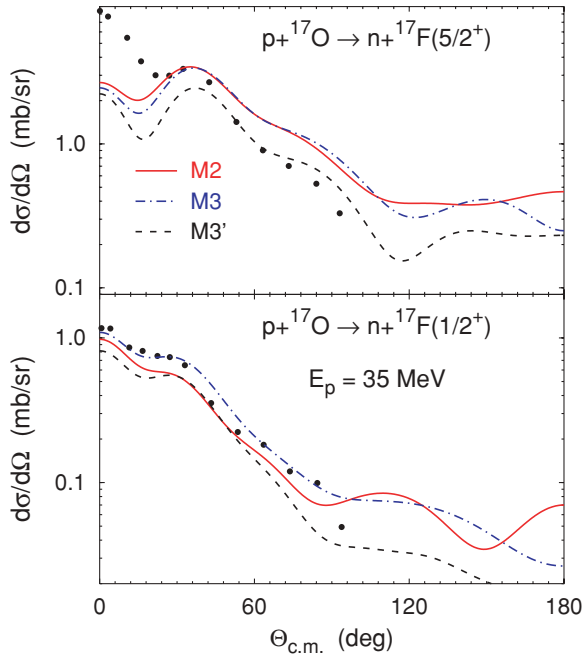

FIG. 11. (Color online) Differential cross section for the $p + {}^{17}\mathrm{O} \to n + {}^{17}\mathrm{F}$ reaction at $E_p = 35$ MeV. Curves are as in Fig. 8. The experimental data are from Ref. [32].

Likewise one may define a distorted wave in channel α as

$$|\tilde{\psi}_\alpha\rangle = (1 + G_\alpha(Z)\,\tilde{T}_\alpha(Z))|\psi_\alpha\rangle. \tag{9}$$

Using the identity

$$G(Z) = \tilde{G}_\beta(Z) + \tilde{G}_\beta(Z)\big[\tilde{G}_\beta^{-1}(Z) - G^{-1}(Z)\big]G(Z), \tag{10}$$

together with Eqs. (1) and (6), one gets

$$G(Z) = \tilde{G}_\beta(Z) + \tilde{G}_\beta(Z)\Omega_\beta G(Z), \tag{11}$$

where

$$\Omega_\beta = \sum_\sigma \bar{\delta}_{\sigma\beta}\,v_\sigma - \tilde{V}_\beta. \tag{12}$$

A new operator $\tilde{U}_{\beta\alpha}(Z)$ relating $G(Z)$ to $\tilde{G}_\alpha(Z)$ instead of $G_\alpha(Z)$, that is,

$$G(Z) = \delta_{\beta\alpha}\tilde{G}_\alpha(Z) + \tilde{G}_\beta(Z)\tilde{U}_{\beta\alpha}(Z)\tilde{G}_\alpha(Z), \tag{13}$$

satisfies an equation

$$\tilde{U}_{\beta\alpha}(Z) = \bar{\delta}_{\beta\alpha}\tilde{G}_\alpha^{-1}(Z) + \Omega_\beta + \Omega_\beta\tilde{G}_\alpha(Z)\tilde{U}_{\alpha\alpha}(Z). \tag{14}$$

Its relation to the standard Faddeev/AGS operator $U_{\beta\alpha}(Z)$ is obtained by using Eq. (7) in Eq. (13) and comparing back with Eq. (3) as

$$U_{\beta\alpha}(Z) = \delta_{\beta\alpha}\,\tilde{T}_\alpha(Z) + \big[1 + \tilde{T}_\beta(Z)\,G_\beta(Z)\big] \times \tilde{U}_{\beta\alpha}(Z)\big[1 + G_\alpha(Z)\,\tilde{T}_\alpha(Z)\big], \tag{15}$$

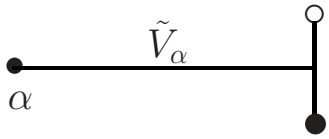

FIG. 12. $\tilde{V}_\alpha$ optical interaction in channel α.

which for on-shell elements reads

$$\langle\psi_\beta|U_{\beta\alpha}(Z)|\psi_\alpha\rangle = \delta_{\beta\alpha}\langle\psi_\beta|\tilde{T}_\alpha(Z)|\psi_\alpha\rangle + \langle\tilde{\psi}_\beta|\tilde{U}_{\beta\alpha}(Z)|\tilde{\psi}_\alpha\rangle. \quad (16)$$

In Eq. (14) the term $\bar{\delta}_{\beta\alpha}\tilde{G}_\alpha^{-1}(Z)$ is zero on-shell and will be omitted in the following considerations.

Using the Born approximation $\tilde{U}_{\beta\alpha}(Z) \simeq \Omega_\beta$ for $\beta \neq \alpha$, one gets

$$\langle\psi_\beta|U_{\beta\alpha}(Z)|\psi_\alpha\rangle \simeq \langle\tilde{\psi}_\beta|\Omega_\beta|\tilde{\psi}_\alpha\rangle, \quad (17)$$

which corresponds to the usual distorted-wave Born approximation (DWBA) for the transfer reactions in the post form.

However, using $\tilde{V}_1 = 0$ in the case of particle 1 colliding with pair (23) one gets $\tilde{T}_\alpha(Z) = 0$, $U_{11}(Z) = \tilde{U}_{11}(Z)$, and $\Omega_1 = v_2 + v_3$, leading to

$$U_{11}(Z) = (v_2 + v_3) + (v_2 + v_3)G_1(Z)U_{11}(Z), \quad (18)$$

which is the integral form of the CDCC differential equation. This equation by itself is not connected in all orders of iteration and therefore cannot be solved by standard numerical methods since it does not satisfy the Fredholm alternative. Nevertheless, one may follow the momentum-space version of the CDCC approach and use the spectral decomposition of $G_1(Z)$ to obtain a set of coupled equations involving the continuum wave functions of pair (23) in addition to the bound-state wave function $|\psi_1\rangle$. If the continuum is discretized and the corresponding wave functions normalized as in CDCC, the solution of Eq. (18) includes the bound to continuum and continuum to continuum couplings that are common to CDCC calculations. In Ref. [14] we have shown that CDCC calculations for deuteron elastic scattering and breakup from a heavier target are reliable, but transfer and breakup reactions involving the scattering of a halo nucleus from a light target, such as $^{11}\mathrm{Be} + p$, may be at fault. Therefore we expect all deuteron elastic scattering results shown in Figs. 1 and 4 to agree well with those obtained from equivalent CDCC calculations.

The present derivations may be useful in future studies of approximate methods often used in nuclear reaction calculations involving deuterons or halo nuclei. Since at this time in the present framework we do not have the means to test the validity of Eq. (17) or any other approximation, we compare our results with published calculations involving either the DWBA, the coupled-channel Born approximation (CCBA), or various adiabatic approaches [33–35]. These calculations use wave functions $|\tilde{\psi}_\alpha\rangle$ and optical potentials $\tilde{V}_\alpha$ that are tuned at the considered reaction energies, whereas our calculations use global fits to nuclear reaction data and are aimed at providing a description of the data in different channels simultaneously. That tuning may be, at least in part, the reason for a better description of the data as discussed in the following.

The data points in Fig. 3 for $p + {}^{13}\mathrm{C} \to d + {}^{12}\mathrm{C}$ were analyzed in Ref. [23] by using the DWBA, the adiabatic deuteron breakup approximation (ADBA), and the CDCC-CCBA. Up to 30° our results coincide with all of the previous calculations, but at larger angles adiabatic and CDCC-CCBA calculations follow the data much better than ours.

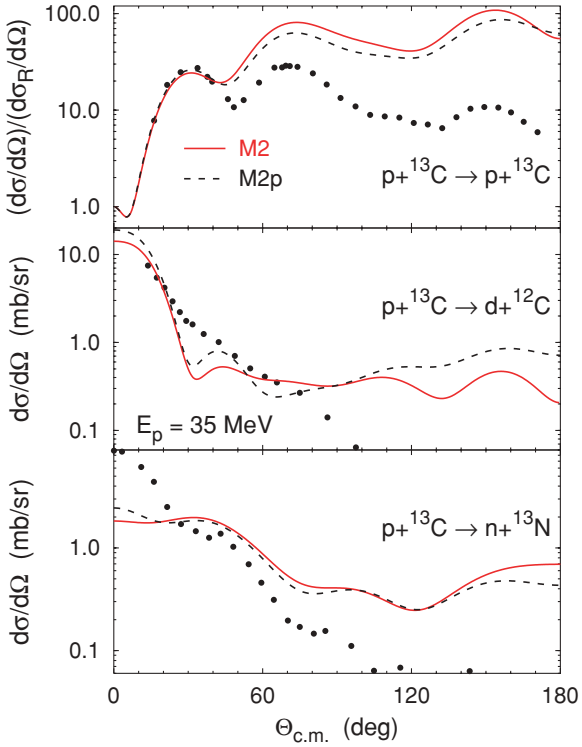

FIG. 13. (Color online) Differential cross section for $p + {}^{13}\mathrm{C}$ elastic and transfer reactions at $E_p = 35$ MeV. Predictions of Model 2 with p-wave potential from Tables I (solid curves) and III (dashed curves) are compared. The experimental data are from Refs. [22,23,31].

Likewise, the data points in Fig. 7 for $d + {}^{12}\mathrm{C} \to p + {}^{13}\mathrm{C}$ were analyzed in Ref. [30] by using the DWBA for transition to the ^{13}C ground state and the CCBA for transitions to the $1/2^+$ and $5/2^+$ excited states. Whereas the DWBA provides a better fit to the data at small angles, it still overshoots the data at larger angles much like our calculations. As for the reactions leading to the $1/2^+$ and $5/2^+$ excited states of ^{13}C, both CCBA and our calculations describe the data equally poorly.

In Ref. [31] the $p + {}^{13}\mathrm{C} \to n + {}^{13}\mathrm{N}$ reaction was analyzed with the DWBA, which undershoots the data at small angles, much like our results shown in Fig. 8, but, overall, provides a better description of the data.

The results in Figs. 9 and 10 for $d + {}^{16}\mathrm{O} \to p + {}^{17}\mathrm{O}$ may be compared with DWBA studies from Ref. [24] and adiabatic calculations from Ref. [35] for 36- and 63.2-MeV deuterons. The results we get in the framework of Model 3 (the "hybrid") are qualitatively similar to those obtained in Refs. [24,35] although quantitatively they may differ in specific angular regions, leading to a description of the data that is not as good as the one provided by DWBA or adiabatic calculations.

Finally, the data in Fig. 11 for $p + {}^{17}\mathrm{O} \to n + {}^{17}\mathrm{F}$ is analyzed in Ref. [32] by using the DWBA. The DWBA calculations leading to the ground state of ^{17}F are qualitatively similar to ours but fit the data better at the forward angles. For the transition to the $1/2^+$ excited state of ^{17}F both calculations are quantitatively similar and fit the data equally well.

V. CONCLUSIONS

We have used the Faddeev/AGS three-body approach to study $d + {}^{12}\mathrm{C}$, $d + {}^{16}\mathrm{O}$, $p + {}^{13}\mathrm{C}$, and $d + {}^{17}\mathrm{O}$ reactions as a three-body system made up by a proton p, a neutron n, and a structureless nuclear core A, the ${}^{12}\mathrm{C}$ or the ${}^{16}\mathrm{O}$. The interactions between pairs are the realistic interactions that describe np, nA, and pA scattering over the relevant energy range. The Coulomb interaction between the proton and the nuclear core is included in a numerically exact (converged) way.

The aim of the present work is to demonstrate the possibilities and the shortcomings of the Faddeev/AGS three-body approach that provides, simultaneously, predictions for all possible reactions, that is, elastic, transfer, and charge-exchange such as, for example, $p + {}^{17}\mathrm{O} \to p + {}^{17}\mathrm{O}$, $p + {}^{17}\mathrm{O} \to d + {}^{16}\mathrm{O}$, and $p + {}^{17}\mathrm{O} \to n + {}^{17}\mathrm{F}$ or $d + {}^{16}\mathrm{O} \to d + {}^{16}\mathrm{O}$, $d + {}^{16}\mathrm{O} \to p + {}^{17}\mathrm{O}$, and $d + {}^{16}\mathrm{O} \to n + {}^{17}\mathrm{F}$.

Three different models (M1, M2, and M3) are studied involving energy-independent and energy-dependent optical potentials that fit the nA and pA elastic scattering and whose parameters are fixed at a chosen energy or are allowed to vary over the energy range of the interacting pair, respectively. In the case of energy-dependent optical potentials these become real at negative energies and support a number of single-particle states that characterize the (An) or the (Ap) nucleus.

The results of our calculations indicate that transfer and charge-exchange reactions at small angles are rather insensitive to the chosen model, but the elastic scattering cross sections are highly sensitive to the choice of energy dependence of the optical interaction (M1 versus M2 and M3). Comparison with published CDCC, DWBA, CCBA, and adiabatic calculations indicates that these approximate methods provide, in general, a better fit of the data than our calculations but are qualitatively similar to our results, particularly the ones of the "hybrid" model M3 that uses a partial-wave-dependent optical potential whose parameters are energy independent except in the partial waves that support the single-particle states of the (An) and (Ap) nuclei.

ACKNOWLEDGMENTS

The authors thank F. M. Nunes and I. J. Thompson for comments on the manuscript. A.D. is supported by Fundação para a Ciência e a Tecnologia (FCT) Grant No. SFRH/BPD/34628/2007 and A.C.F. in part by FCT Grant No. POCTI/ISFL/2/275.

APPENDIX

We present here selected results obtained with an alternative N-${}^{12}\mathrm{C}$ p-wave potential whose spin-orbit strength is the same as in the other partial waves (see Table I). The strength of the central part is adjusted to reproduce ${}^{13}\mathrm{C}$ and ${}^{13}\mathrm{N}1p_{1/2}$ ground-state energies as in Table II, thereby resulting in different binding energies for the Pauli forbidden $1p_{3/2}$ bound states. These are given in Table III together with the new values of potential parameters.

The predictions of Model 2 with p-wave potential from Tables I and III are compared in Fig. 13 for $p + {}^{13}\mathrm{C}$ elastic and transfer reactions. The differences are rather insignificant when compared to the discrepancies between theory and data and therefore do not change the conclusions of this paper. Differences of similar magnitude can also be seen for the observables of $d + {}^{12}\mathrm{C}$ reactions.

TABLE III. Parameters of the alternative N-${}^{12}\mathrm{C}$ p-wave potential together with the resulting binding energies for the Pauli forbidden $1p_{3/2}$ bound state. See Tables I and II for further explanation.

$v_R(nA)$	$v_R(pA)$	$V_{\mathrm{so}}(NA)$	$1p_{3/2}({}^{13}\mathrm{C})$	$1p_{3/2}({}^{13}\mathrm{N})$
49.61	49.11	5.5	8.587*	5.507*

[1] N. Austern, Y. Iseri, M. Kamimura, M. Kawai, G. Rawitscher, and M. Yahiro, Phys. Rep. **154**, 125 (1987).
[2] S. T. Butler, Proc. R. Soc. London A **208**, 559 (1951).
[3] L. D. Faddeev, Zh. Eksp. Teor. Fiz. **39**, 1459 (1960) [Sov. Phys. JETP **12**, 1014 (1961)].
[4] E. O. Alt, P. Grassberger, and W. Sandhas, Nucl. Phys. **B2**, 167 (1967).
[5] W. Glöckle, *The Quantum Mechanical Few-Body Problem* (Springer-Verlag, Berlin/Heidelberg, 1983).
[6] B. A. Watson, P. P. Singh, and R. E. Segel, Phys. Rev. **182**, 978 (1969).
[7] R. Machleidt, Phys. Rev. C **63**, 024001 (2001).
[8] R. Aaron and P. E. Shanley, Phys. Rev. **142**, 608 (1966).
[9] E. O. Alt, L. D. Blokhintsev, A. M. Mukhamedzhanov, and A. I. Sattarov, Phys. Rev. C **75**, 054003 (2007).
[10] A. Deltuva, A. C. Fonseca, and P. U. Sauer, Phys. Rev. C **71**, 054005 (2005); **72**, 054004 (2005); **73**, 057001 (2006).
[11] A. Deltuva, A. C. Fonseca, and P. U. Sauer, Phys. Rev. Lett. **95**, 092301 (2005).
[12] J. R. Taylor, Nuovo Cimento B **23**, 313 (1974); M. D. Semon and J. R. Taylor, Nuovo Cimento A **26**, 48 (1975).
[13] E. O. Alt, W. Sandhas, and H. Ziegelmann, Phys. Rev. C **17**, 1981 (1978); E. O. Alt and W. Sandhas, *ibid.* **21**, 1733 (1980).
[14] A. Deltuva, A. M. Moro, E. Cravo, F. M. Nunes, and A. C. Fonseca, Phys. Rev. C **76**, 064602 (2007).
[15] R. Crespo, E. Cravo, A. Deltuva, M. Rodríguez-Gallardo, and A. C. Fonseca, Phys. Rev. C **76**, 014620 (2007).
[16] R. Crespo, A. Deltuva, E. Cravo, M. Rodríguez-Gallardo, and A. C. Fonseca, Phys. Rev. C **77**, 024601 (2008).
[17] K. Chmielewski, A. Deltuva, A. C. Fonseca, S. Nemoto, and P. U. Sauer, Phys. Rev. C **67**, 014002 (2003).
[18] A. Deltuva, K. Chmielewski, and P. U. Sauer, Phys. Rev. C **67**, 034001 (2003).
[19] A. Deltuva, A. C. Fonseca, and P. U. Sauer, Annu. Rev. Nucl. Part. Sci. **58**, 27 (2008).
[20] A. Deltuva, Phys. Rev. C **74**, 064001 (2006).
[21] G. Perrin, N. Van Sen, J. Arvieux, R. Darves-Blanc, J. L. Durand, A. Fiore, J. C. Gondrand, F. Merchez, and C. Perrin, Nucl. Phys. **A282**, 221 (1977).

[22] E. Fabrici, S. Micheletti, M. Pignanelli, F. G. Resmini, R. De Leo, G. D'Erasmo, and A. Pantaleo, Phys. Rev. C **21**, 844 (1980).
[23] H. Toyokawa, H. Ohnuma, Y. Tajima, T. Niizeki, Y. Honjo, S. Tomita, K. Ohkushi, M. H. Tanaka, K. Kubono, and M. Yosoi, Phys. Rev. C **51**, 2592 (1995).
[24] M. D. Cooper, W. F. Hornyak, and P. G. Roos, Nucl. Phys. **A218**, 249 (1974).
[25] E. Newman, L. C. Becker, B. M. Preedom, and J. C. Hiebert, Nucl. Phys. **A100**, 225 (1967).
[26] H. Feshbach, *Theoretical Nuclear Physics: Nuclear Reactions* (Wiley, New York, 1992).
[27] W. N. Polyzou and E. F. Redish, Ann. Phys. (NY) **119**, 1 (1979).
[28] A. Deltuva, K. Chmielewski, and P. U. Sauer, Phys. Rev. C **67**, 054004 (2003).
[29] A. Deltuva, A. C. Fonseca, and P. U. Sauer, Phys. Lett. **B660**, 471 (2008).
[30] H. Ohnuma *et al.*, Nucl. Phys. **A448**, 205 (1986).
[31] H. Ohnuma *et al.*, Nucl. Phys. **A456**, 61 (1986).
[32] M. Oura *et al.*, Nucl. Phys. **A586**, 20 (1995).
[33] R. C. Johnson and P. J. R. Soper, Phys. Rev. C **1**, 976 (1970).
[34] R. C. Johnson, J. S. Al-Khalili, and J. A. Tostevin, Phys. Rev. Lett. **79**, 2771 (1997).
[35] N. K. Timofeyuk and R. C. Johnson, Phys. Rev. C **59**, 1545 (1999).